Industrial Chemistry & Materials

ROYAL SOCIETY OF CHEMISTRY

PAPER

View Article Online
View Journal

Cite this: DOI: 10.1039/d5im00045a

Sorption-enhanced DME synthesis provides high flexibility: evidence from modelling four industrial use cases†

Ioannis Tyraskis, Alma Capa, * Galina Skorikova, Soraya N. Sluijter and Jurriaan Boon

Sorption-enhanced dimethyl ether synthesis (SEDMES) is a powerful technology to produce dimethyl ether (DME) from residual industrial gas streams or captured CO_2 and renewable H_2. *In situ* water removal by zeolites shifts the thermodynamic equilibrium of the reaction towards product formation. Sorption enhancement proved to provide a single-pass CO_2 conversion above state of the art values. Building knowledge on prior optimisation of a CO_2–H_2 feed, this work extends modelling of SEDMES to a design study for four distinct industrial feeds, with progressively higher CO content. The trade-offs between DME productivity and carbon distribution over the products were studied. The impact of process parameters such as cycle duration, feed flow, operating pressure, temperature, reactant stoichiometry, amount of inert gases and the presence of CO was analysed in detail, including the impact of flexible operation and turndown. Results show that higher CO feed concentrations enhance the DME productivity but complicate the purification due to increased CO_2 by-product formation. Variations in the feed H_2–C ratio affected by-product selectivity, with lower ratios reducing CO_2 and methanol formation, potentially simplifying downstream processing. Pressure and temperature were identified as critical design parameters. Higher operating pressures consistently enhanced DME productivity in all cases, while a moderate temperature increase above 250 °C proved to be beneficial as well. Moreover, the process demonstrated resilience under lower feed flow conditions (factor 3 in turn down ratio) that could potentially be caused by renewable electricity fluctuations, without compromising the performance.

Keywords: Dimethyl ether; CO_2 utilisation; Modelling; Sorption enhanced reaction; Pressure-swing adsorption (PSA); Syngas.

Received 31st March 2025,
Accepted 9th July 2025

DOI: 10.1039/d5im00045a

rsc.li/icm

1 Introduction

Dimethyl ether (DME), the simplest ether and the dehydrated form of methanol, is emerging as a promising new generation alternative fuel, platform chemical and hydrogen carrier that could play an important role in the energy transition.[1] Comparing DME with MeOH, it has a higher calorific value meaning more energy is generated in its combustion process.[2] DME has a low auto-ignition temperature, is an oxygenated fuel with no C–C bonds in the molecular structure leading to reduced soot formation and has good air–fuel mixing properties preventing particulate formation. In addition, with a properly designed DME injection and combustion system nitrogen oxide (NOx) emissions can be reduced. These characteristics make DME an ideal diesel-cycle fuel.[3–6] DME was also found to be a good gas turbine fuel with emission properties comparable to natural gas allowing performance improvement through thermochemical recuperation and decrease of the specific CO_2 emissions.[4,7]

Conventionally, DME is produced in a two-step process identified as the indirect DME synthesis route.[1,2,8,9] In a first reactor methanol is synthesised from CO_2 and/or CO followed by methanol dehydration to DME in a separate reactor. The complete set of reactions is as follows (eqn (1)–(4)):

Methanol synthesis

$$CO_2 + 3H_2 \leftrightarrow CH_3OH + H_2O \quad \Delta H_r^0 = -49\ \text{kJ mol}^{-1} \qquad (1)$$

$$CO + 2H_2 \leftrightarrow CH_3OH \quad \Delta H_r^0 = -90\ \text{kJ mol}^{-1} \qquad (2)$$

Water gas shift

Sustainable Technologies for Industrial Processes, Energy & Material Transition, TNO, Petten, The Netherlands. E-mail: alma.capatamargo@tno.nl

† Electronic supplementary information (ESI) available. See DOI: https://doi.org/10.1039/d5im00045a

$$CO + H_2O \leftrightarrow CO_2 + H_2 \quad \Delta H_r^0 = -41 \text{ kJ mol}^{-1} \tag{3}$$

Methanol dehydration

$$2CH_3OH \leftrightarrow CH_3OCH_3 + H_2O \quad \Delta H_r^0 = -24 \text{ kJ mol}^{-1} \tag{4}$$

On the other hand, direct synthesis of DME can be defined as an one-step synthesis which can be an alternative pathway of the previous two-step synthesis process. In this process the hydrogenation (eqn (1) and (2)) and the dehydration (eqn (4)) will take place in a single reactor together with the (reverse) water gas shift reaction (eqn (3)). The direct DME synthesis benefits from the continuous conversion of one of the intermediates, MeOH, shifting the equilibrium towards DME production.[2,8,10,11] Since the reaction is still equilibrium limited, downstream separation produces large recycle streams of syngas, CO_2 and methanol. Steam separation enhancement is shown to be a promising route for CO_2 conversion. This is because in direct DME synthesis CO is converted to DME with CO_2 as the major by-product and with increasing CO_2 content in the feed both the conversion and the selectivity towards DME decrease significantly. In contrast, this is not the case for sorption enhanced DME synthesis which has been shown to have a highly selective direct conversion of CO_2 to DME. As a result, both the carbon conversion and the DME selectivity are far higher for the SEDMES process compared to the direct DME synthesis, especially for a CO_2-rich feed.[1] In principle steam separation enhanced DME synthesis can be obtained using selective membranes or *in situ* adsorption. The membrane separation has the advantage to work at steady-state, while a cyclic regeneration of the adsorbent material is needed in reactive adsorption. This second solution is anyway more suitable, since low water partial pressure must be reached in the reactor for a substantial enhancement of the DME synthesis process and water removal in the membrane is effective only with a consistent partial pressure gradient (indicatively >1 bar).[12] Therefore, the CO_2 conversion using membrane reactors is higher than that of a traditional reactor reporting a DME yield up to 54.5% and a single-pass CO_2 conversion up to 73.4%.[13,14]

The sorption enhanced DME synthesis (SEDMES) technology is a novel process for the production of DME in which water is removed *in situ* by the use of a solid adsorbent, typically a LTA zeolite, enhancing the reactant conversion as stated by the Le Chatelier's principle. By the removal of water as a reaction product, the oxygen surplus of the feed no longer ends up in CO_2, as is the case for the direct DME synthesis, but in (adsorbed) H_2O instead.[1,15] The SEDMES concept has been evaluated not only by modelling the process[1,12,15,16] but also experimentally, proving that DME yield and DME selectivity are improved over conventional processes showing DME yields of at least 80%.[16–21] Even though a catalytic membrane reactor can achieve a single-pass carbon conversion up to 73.4% the SEDMES process can be very versatile and the single-pass carbon conversion can be above 75%. SEDMES combines the chemical reaction and adsorption in one process. Therefore, it is a reactive adsorption process operated in cycles of consecutive reactive adsorption and adsorbent regeneration. The regeneration of the adsorbent is key for the efficiency of the process.[15,22] In a first experimental study it was concluded that the combined temperature and pressure swing adsorption (TPSA) results in very high DME yields; in a more recent study, in which SEDMES had been tested under industrially-relevant conditions, similar conversion and selectivity were obtained with pressure swing adsorption (PSA). Since the potentially faster and more energy efficient approach is PSA, the preferred operation for SEDMES is as a PSA process. Due to the high yield that the SEDMES technology can achieve, it is a very promising technology for the production of renewable DME.

The production of carbon neutral fuels and synthetic hydrocarbons such as MeOH or DME by recycling CO_2 from industrial sources or even from the air itself is receiving increasing attention.[23] In particular, three types of use cases for the production of DME seem particularly relevant and will be further investigated in this work: captured CO_2 from biogenic or nonbiogenic origin, the use of residual steel gases, and gasified waste streams. Firstly, the industrial energy transition will require the conversion of substantial amounts of captured CO_2, either from point sources such as cement production and natural gas processing, or from air.[24,25] In these cases, the DME synthesis will be performed using a (nearly) pure CO_2 stream combined with a stoichiometric amount of renewable hydrogen.

Secondly, research has been done on the conversion of by-product gas from the steel-making process into valuable chemicals for either CO_2 reduction or increasing energy efficiency.[26] Most of these studies are devoted to MeOH[27–31] but attention to its dehydrated form, DME, is increasing. For example, Park *et al.* compared the single and two-step processes for the synthesis of DME using the by-product gas from a steel mill. The authors concluded that although the single-step reactor showed a better production rate and energy efficiency, further study on the techno-economic analysis for both processes is needed.[32] Jeon *et al.* studied a DME synthesis process using steelmaking by-product gases demonstrating that the application of DME production in the steelworks industry could be an effective strategy for the reduction of CO_2 emissions.[33] A demonstrator pilot was tested in the frame of the H2020 C2Fuel project in which CO_2 was removed from steel off-gases and sent to a DME production unit.[34] Even though interest is increasing, research about DME production from steelworks arising gases is still limited, especially for intensified DME production processes. Therefore, one of the use cases studied in this work is the production of renewable DME from steel off-gas *via* SEDMES. Thirdly, besides feedstocks that are CO_2-rich DME can also be produced from synthesis gas (syngas) which is a mixture of H_2, CO and CO_2. The use of biomass or municipal solid waste as feedstock to produce transportation

fuels and chemicals is a central policy to address environmental and oil dependence issues of today's society.[17] Biomass can be gasified to produce syngas which can be burnt in gas turbines like natural gas or it can be converted to high quality chemicals and fuels, such as methanol and DME.[35] The production of bio-DME is being investigated by different research groups. Different biomass resources can be used for the ultimate production of bio-DME.[36–39] The production of DME from digestate-derived syngas,[40] landfill gas or biogas[41–43] or from syngas in the Kraft pulp process[44] has also been explored in the literature. Some initiatives that include the bio-DME synthesis are already at a pilot scale. For example, the Bioliq process developed at the Karlsruhe Institute of Technology (KIT) aims to convert biomass residues into synthetic fuels *via* DME in a pilot plant with a thermal fuel conversion capacity of 2–5 MW.[45] The combination of biomass gasification and hydrogen from electrolysis for the production of DME is also gaining interest among the research community.[36,46–48] However, most of these studies are focused on conventional DME synthesis routes having limited single-step conversions due to the thermodynamic limitations of the conventional DME synthesis processes. The Horizon 2020 FLEDGED (flexible DME production from biomass) investigated the production of DME *via* sorption enhanced gasification (SEG) of second generation biomass (such as wood and MSW) aiming to develop technologies (TRL5) leading to process intensification and cost reduction of the biomass-to-DME conversion process.[49,50] In the FLEDGED project not only intensified gasification was explored but also, intensified DME synthesis using sorption enhanced DME synthesis (SEDMES) technology.[1,12,17,20] SEDMES experiments from mixtures of H_2, CO and CO_2 showed an increased yield of DME, an improved selectivity to DME over methanol, and strongly reduced CO_2 content in the product. However, there are still some research questions to be answered (*i.e.*, DME selectivity and productivity trade off, optimum cycle time for a given cycle design, *etc.*). Therefore, the bio-DME production *via* SEDMES is also included in this work as a use case in order to build knowledge on those uncertainties.

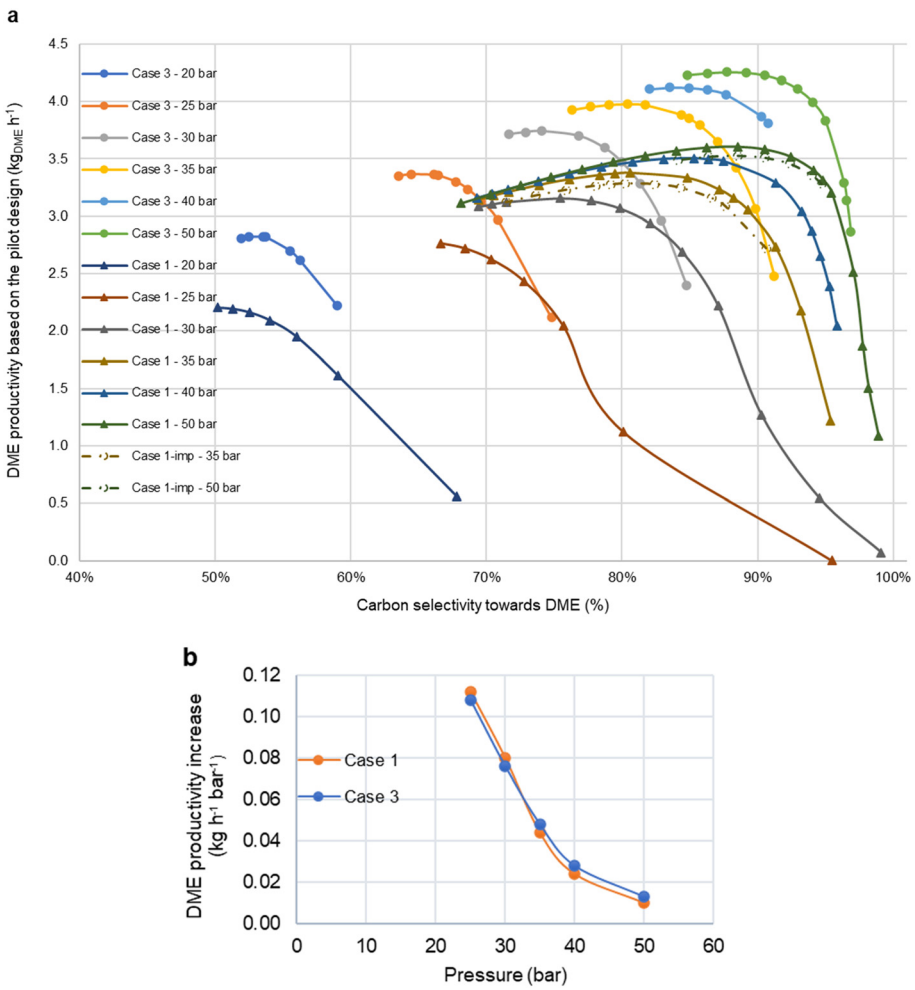

Fig. 1 Comparison of DME productivity and selectivity for cases 1 and 3, for different operating pressures and cycle durations (cycle duration increases while moving to lower carbon selectivity) (a); rate of DME productivity increase per unit of pressure (b); the reaction temperature is 250 °C.

The objective of this work is to analyse the flexibility that SEDMES provides for the production of renewable DME from feedstocks from different industrial use cases like natural gas cleaning, indirect biomass gasification and steel off-gases. As explained before, SEDMES operates in cycles between reactive adsorption and adsorbent regeneration. The cycle design that operates at the largest dedicated SEDMES installation at TNO Petten, The Netherlands, is used as reference for the modelling of the different use cases. The cycle design is detailed in the methodology section. The main developments associated with this technology are related to process optimisation and scaling-up.[51] Therefore, in addition to the flexibility analysis, this paper is building knowledge on the process optimisation by reporting for the first time Pareto plots obtained for the aforementioned industrial use cases where a trade-off between *C*-selectivity towards DME and DME productivity is analysed.

2 Results and discussion

2.1 Effect of feed composition on DME selectivity and productivity

In previous studies, increased pressure was shown to enhance the performance of the SEDMES process both in terms of productivity and selectivity.[1,52] In the current study, this was found to be consistent across all CO/CO_2 feed ratios. However, variations in the performance were observed between different cases, with the degree of enhancement depending on the specific feed composition.

In Fig. 1a, case 3 (steel off-gas) is compared with case 1 (natural gas cleaning). The graph shows that the inclusion of CO in the feed, in equal molar amounts as CO_2, corresponding to case 3, leads to higher DME productivities. This increase is attributable to the fact that the conversion of CO to DME does not generate water in the methanol synthesis step (eqn (2)), so the amount of water in the reaction product is lower and the column would be in drier conditions which is beneficial for the system since water accumulation is reduced (see purge profiles in Fig. 2a in the annex). Numerous studies have experimentally confirmed that CO_2 negatively affects both the thermodynamics and kinetics of the process.[53–58] This effect has been attributed in the literature to the WGS equilibrium (eqn (3)). Increasing the CO_2 concentration (case study 1) leads to the promotion of the reverse water-gas shift (r-WGS) reaction causing H_2O accumulation in the reaction environment that has a detrimental effect on CO_2 hydrogenation (eqn (1)) and methanol dehydration (eqn (4)).[59] In addition the CO_2 hydrogenation reaction produces water but during CO hydrogenation water is not produced.

The productivity peaks for each pressure curve correspond to similar selectivity ranges for both cases. However, a closer examination reveals that at 20 bar, the productivity peak for case 3 (2.8 kg h^{-1} at 54% DME selectivity) occurs at a higher selectivity compared to case 1 (2.2 kg h^{-1} at 50% DME selectivity). For all other pressures, the differences in selectivity are minimal. The same selectivity trend is observed later in cases 2 and 4 (indirect biomass gasification). The productivity peak at 50 bar was achieved at a DME selectivity of 89.1% for case 3 and 88.5% for case 1, with a productivity of 4.25 kg h^{-1} and 3.60 kg h^{-1}, respectively. To produce a DME product with almost the same purity, case 3 required 606 mol h^{-1} H_2, 156 mol h^{-1} CO, and 98 mol h^{-1} CO_2, whereas case 1 required 661 mol h^{-1} H_2 and 220 mol h^{-1} CO_2. After adjusting for capacity differences, the optimal performance at 50 bar necessitates 143 mol kg^{-1} h^{-1} H_2, 37 mol kg^{-1} h^{-1} CO, and 23 mol kg^{-1} h^{-1} CO_2 for case 3, and 184 mol kg^{-1} h^{-1} H_2 and 61 mol kg^{-1} h^{-1} CO_2 for case 1. Therefore, the case in which the recovery of steel off-gases is studied (case 3) has a more efficient utilisation of H_2.

Case 1 exhibits a slightly more pronounced decline in the rate of productivity increase as pressure rises, which is depicted in Fig. 1b. At 25 bar, the productivity gain per unit of pressure is higher in case 1 (0.112 kg h^{-1} bar^{-1}) compared to case 3 (0.108 kg h^{-1} bar^{-1}). However, at 50 bar, this trend reverses, with the productivity increase per unit of pressure in case 1 estimated to be 77% lower, resulting in only a 0.01 kg h^{-1} increase per additional bar, compared to 0.013 kg h^{-1} in case 3. This effect aligns with the findings of van Kampen *et al.*,[1] who showed that increasing pressure favours CO conversion more than CO_2 conversion. This effect could be

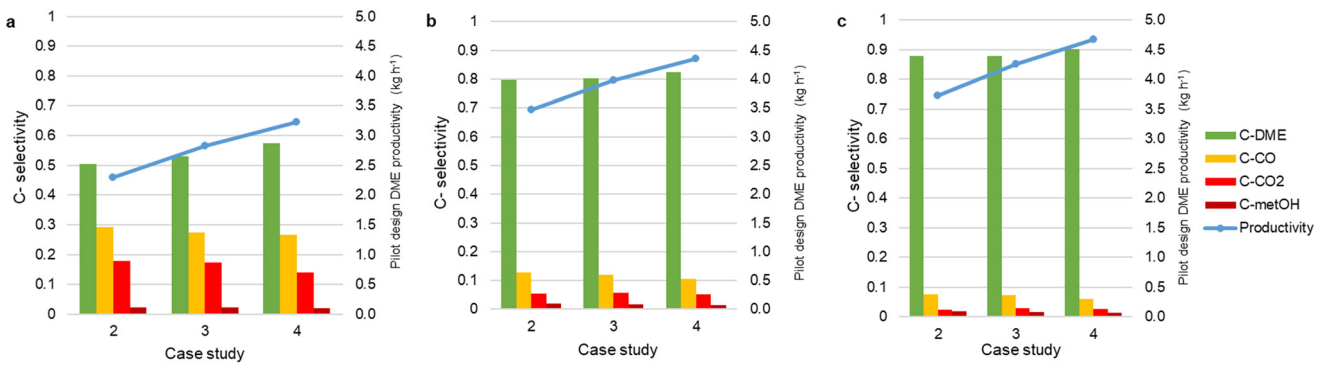

Fig. 2 Carbon selectivity and DME productivity of the maximum productivity operational points for cases 2, 3 and 4 at 20 (a), 35 (b) and 50 (c) bar.

explained by the Le Chatelier's principle which could be more pronounced for the CO conversion having a greater impact by the pressure on that reaction compared to the CO_2 conversion: methanol synthesis from both CO and CO_2 is a shrinking reaction while the reduction in number of moles when starting from CO_2 (eqn (1)) is a factor 2 whereas when starting from CO it is a factor 3 (eqn (2)).

Analysis of different sets of CO/CO_2 concentrations in the feed corroborates the findings presented in Fig. 1. Cases 2, 3, and 4 exhibit a gradually increasing CO/CO_2 ratio of 0.17, 1.02, and 3.24, respectively. Fig. 2 displays the performance at the maximum productivity peaks, at three different operating pressures: 20, 35, and 50 bar. Similar to our previous work, comparing maximum productivity peaks serves as a reference point considered within the optimal performance range for typical process designs.[52] The results demonstrate that increasing the CO concentration in the feed enhances the productivity of the SEDMES process, as expected. Interestingly, DME selectivity also shows a slight improvement (~4%) with higher CO content in the feed at 20 bar; however, this effect becomes less apparent at higher pressures. This is attributed to the fact that DME formation as a shrinking reaction highly benefits from the increase in pressure, while an equimolar r-WGS reaction is not affected by it. Consequently, in the lower pressure region the competition of r-WGS reaction increases. As presented by Jia *et al.*, direct hydrogenation of CO bypasses this side r-WGS reaction.[60] As a result, introduction of CO and reduction of CO_2 in the feed minimises by-product formation at lower pressures and maintains more consistent DME selectivity increase across the pressure range.

Table 1 presents the DME productivity and selectivity values at maximum productivity operations for both 35 and 50 bar, along with the required reactant flow to produce 1 kg h^{-1} of DME. At both pressure levels, case 4 (indirect gasification case with higher CO content) exhibited markedly higher DME productivity and slightly higher DME selectivity compared to the other cases. DME productivity demonstrated an almost linear increase with higher CO content in the feed. DME selectivity generally remained within similar ranges; however, there appeared to be a slight improvement with increased CO content. Notably, case 2, which contained 5.7 mol% CO, exhibited a minor decrease in selectivity compared to case 1, followed by an increase in selectivity in cases 3 and 4. These trends were consistent across both pressure levels, indicating that an increase in CO content must exceed a certain threshold to enhance carbon selectivity towards DME. Conversely, a high CO_2 content will give rise to a reduction in the CO conversion. Indeed, Jia *et al.*[60] have observed that the net CO conversion (the difference between the conversion of CO by methanol synthesis and the production of CO *via* reverse water-gas shift) drops significantly upon increasing the CO_2 content in the feed. Additionally, the carbon conversion to DME is also shown in Table 1. This parameter follows a similar tendency to the DME selectivity and productivity and is calculated using eqn (18).

Increasing the feed CO content up to 26.2 mol% in case 4 significantly enhances the SEDMES process by boosting both DME productivity and selectivity. Compared to the CO-free case 1 (including inerts), case 4 showed a 32% increase in productivity compared to case 1 at both 35 and 50 bar operation, reaching 4.67 kg h^{-1} in the latter. At the productivity peaks, the corresponding DME selectivity was slightly increased by 2.7% and 1.7% at 35 and 50 bars, respectively. Additionally, case 4 achieves these gains while requiring up to 30% less H_2 in the feed, improving the overall economic efficiency of the process. Notably, longer cycle durations extend the duration of all process steps, including the purge, which is particularly relevant for high-performing conditions since the column is drier, characterised by high pressures and high CO content like case 4 for the indirect gasification scenarios, or case 3 for the industrial steel off-gases. If H_2 is used in the purge, this would result in higher hydrogen consumption. However, it is assumed that purge gas will be recycled in large-scale designs *via* a purge loop, a factor not yet included in the current model but being implemented at the pilot scale.

Diving deeper in the effect of CO content in SEDMES operation, the productivity–selectivity graphs for all cases at 35 bar are analysed in Fig. 3a. All curves exhibit a similar trend: higher CO content in the feed allows for operation at higher productivity levels without changing the *M*-module in the feed. The graph indicates that curves representing higher CO/CO_2 ratios are steeper and intersect those with lower CO/CO_2 ratios. This happens because higher CO_2 content will result in larger generation of water during the methanol

Table 1 Overview of the performance of all cases at 35 and 50 bar

		35 bar					50 bar				
		Case 1					Case 1				
		No inert	Inert	Case 2	Case 3	Case 4	No inert	Inert	Case 2	Case 3	Case 4
CO content in feed (mol%)		0.0	0.0	5.7	17.7	26.2	0.0	0.0	5.7	17.7	26.2
Productivity (kg_{DME} h^{-1})		3.38	3.28	3.46	3.98	4.35	3.6	3.53	3.72	4.25	4.67
DME selectivity (%)		80.6	80.3	79.7	80.4	82.5	88.5	88.5	87.9	89.1	90.0
Reactant flow (mol kg_{DME} h^{-1})	H_2:	195	197	187	52	139	184	184	174	143	129
	CO:	0	0	14	39	53	0	0	13	37	49
	CO_2:	65	65	53	24	10	61	61	49	23	10
Cycle duration (min)		172.5	172.5	180	195	210	232.5	232.5	240	255	300
Carbon conversion to DME (%)		71	71	71	74	78	78	78	78	81	84

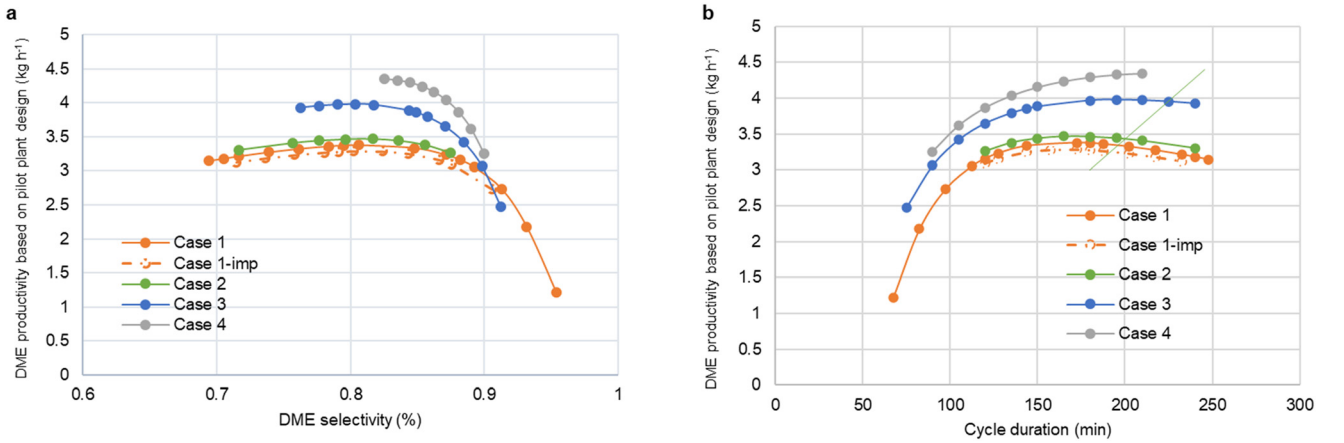

Fig. 3 Pareto plot of DME productivity *vs.* DME selectivity with lower DME selectivity (left side of the *x*-axis) corresponding to increasing cycle duration (a); DME productivity against cycle duration showing the maximum operating points with the green line (b). Dashed lines show the performance of case 1 in case it contained a similar level of impurities to the other cases.

synthesis step and faster hold up in the sorbent, which will reduce the increase rate in productivity while cycle duration increases.[12] This suggests that as the CO content in the feed increases, the DME selectivity range corresponding to maximum productivity (optimal operation) narrows. Consequently, in optimal DME selectivity ranges, the performance of the SEDMES process is more strongly influenced by changes in cycle duration when the CO content in the feed is higher. The maximum productivity operating points for all cases are provided in the aforementioned Table 1.

Cycle duration is a critical parameter for the optimal operation of the process, influenced by both flow composition and flow rate. As is already known, an increase in pressure necessitates a longer cycle duration for optimal performance.[52] In the current study, increasing the CO/CO_2 ratio also resulted in longer cycle durations to achieve maximum productivity. This is attributed to the fact that water production per mole of DME is lower when CO is used as the carbon source, compared to CO_2, which slows down water accumulation. Consequently, and in accordance with the findings of Guffanti *et al.*,[12] the higher water loading in CO_2-rich conditions necessitates more frequent or longer regeneration of the adsorbent material to prevent saturation. As depicted in Fig. 3b for 35 bar pressure, the optimal operating region – where productivity peaks are achieved – shifts to longer cycle durations as the CO/CO_2 ratio increases. The specific cycle durations corresponding to each productivity peak are presented in Table 1, along with the values for 50 bar, which exhibit a similar trend.

2.2 Effect of different process parameters on by-product selectivity

2.2.1 Effect of the CO/CO_2 feed ratio. In the previous chapter, we assessed all cases in terms of productivity and selectivity to DME. The next step involves comparing them based on the selectivity to side-products, which is presented in Fig. 4. The final product compositions across the different cases exhibit only minor differences. The outcomes for case 2 (indirect gasification case with a lower CO amount) closely resemble those of case 1 (natural gas cleaning without CO). However, the influence of CO in the feed is particularly evident in cases 3 and 4 (steel off-gas and indirect gasification with higher CO content). There is a discernible

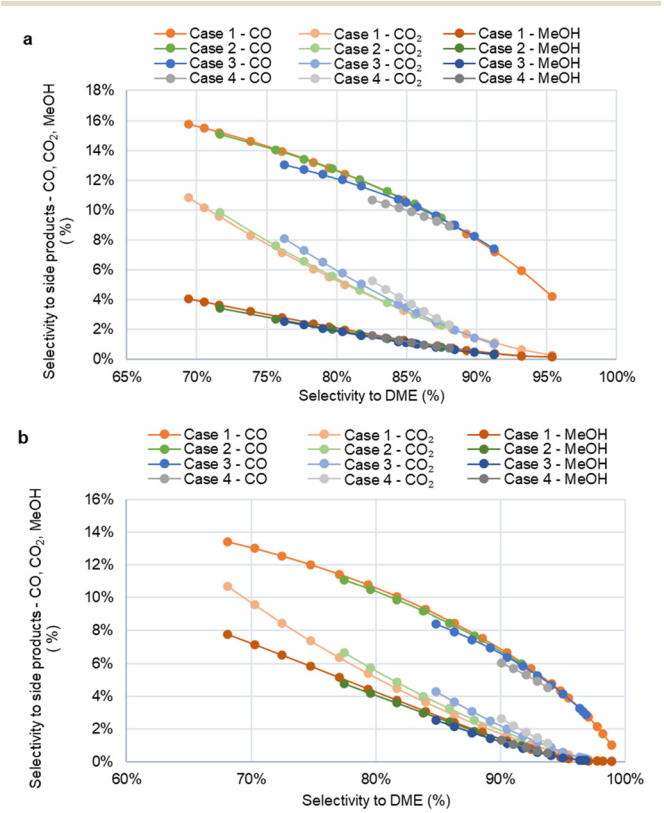

Fig. 4 Comparison of by-product selectivity for all cases at 35 bar (a) and 50 bar (b), plotted against DME selectivity.

trade-off between CO and CO_2 selectivity, with a reduction in CO selectivity and a corresponding increase in CO_2 selectivity at specific DME selectivity below 90%. Case 4 demonstrates the most pronounced trade-off, with a selectivity difference of up to 1% compared to case 1 (which has no CO content in the feed) at a DME selectivity of 82%. Case 3 shows a slightly lower degree of this trade-off. MeOH selectivity increases with lower CO content, but to a very small degree that is not clearly visible in the diagram. The observed behaviour of by-product selectivity with varying feed compositions is closely linked to water accumulation and the WGS system. Despite the active water removal from the system, WGS shift reaction occurs and becomes more profound when sorbent saturation is reached.[59] Cases with high CO content shift the equilibrium towards CO_2 formation.[8,17] Conversely, cases rich in CO_2 promote r-WGS reaction which increases carbon selectivity to CO. As a result, despite starting with higher content of CO_2 in the feed, they result in lower CO_2 and higher CO content in the product, when comparing the same DME selectivity levels.

Higher DME selectivity, shown on the *x*-axis of Fig. 4a, are achieved at shorter cycle durations, where accumulation is minimal and the sorbent has not yet reached saturation. Within this range, there is no significant difference in product selectivity among the cases. However, as DME selectivity approaches the 85% range—corresponding to the maximum productivity range shown in Fig. 4b—the impact of sorbent saturation becomes more pronounced.

As previously reported in the literature, the separation of CO_2 from DME is the most challenging aspect of purifying the SEMDES product, due to the high affinity between the compounds, but its recycle is necessary to minimise losses. In contrast, excess CO can be more easily recycled back into the process using a flash drum.[8,22,61] Consequently, the presence of CO in the feed slightly complicates the downstream processing of DME production, as it leads to higher CO_2 content in the product, thereby increasing the energy requirements for purification. Fig. 4b further explores this effect at 50 bar pressure, revealing similar trends across cases 3 to 4 but with noticeable differences in by-product selectivity compared to the 35 bar scenario. Specifically, at 50 bars, CO selectivity decreases, while MeOH selectivity clearly increases, with the MeOH selectivity curves positioned closer to the CO_2 selectivity curves. Meanwhile, the CO_2 selectivity remains relatively unchanged across all cases. This observation might be associated with the effect of the pressure, according to Le Chatelier's principle, on the CO hydrogenation reaction (eqn (2)). However, a direct comparison between the two graphs is challenging, because 50 bar operation necessitates larger cycle duration, and thus more water accumulation to achieve comparable DME selectivity – below its maximum productivity peak – to the 35 bar operation. Hence, the aforementioned differences in by-product selectivity are primarily driven by the higher water content in the reactor. For a clearer visualisation of this effect, Fig. 3a in the Annex plots the by-product selectivity

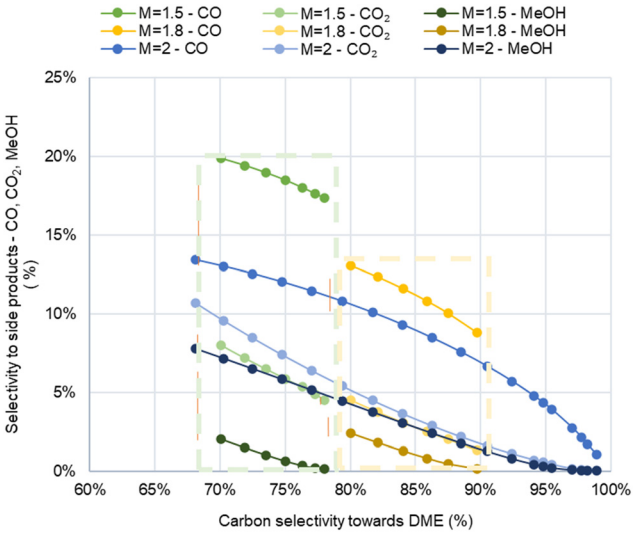

Fig. 5 Selectivity to by-products *versus* DME selectivity for case 1 across varying *M*-modules.

ratios for the productivity peaks of case 1 at pressures of 20, 35, and 50 bar. Between 20 and 50 bar pressure, the ratios of MeOH/CO, MeOH/CO_2, and CO/CO_2 increase by 3.1, 4.5 and 1.5 times, respectively. The same trend of increasing carbon-to-methanol selectivity with increasing pressure can also be observed in cases 2, 3, and 4, as shown before in Fig. 2.

2.2.2 Effect of the *M*-module. The performance of case 1 was further analysed across various *M*-modules, revealing a pattern similar to the one observed when reducing CO content in the feed. As illustrated in Fig. 5, a comparison of M = 1.5, M = 1.8, and M = 2 at 50 bar clearly shows that reduced *M*-modules lead to significantly lower by-product formation across the entire DME selectivity range. For instance, at M = 1.5, CO_2 and MeOH selectivity decrease by 1.6% and 5.1%, respectively, while CO selectivity rises by 6.8%, compared to M = 2. These changes in by-product selectivity are notably more pronounced than those resulting from variations in CO content in the feed, as discussed earlier. This difference is attributed to two factors. Firstly, the substoichiometric operation that requires shorter cycle durations to achieve the same DME selectivity, along with a reduced water production rate. As a result, water accumulation and sorbent saturation are minimised, leading to a lower water concentration. Secondly, as demonstrated by Jia *et al.*,[60] the higher concentrations of CO_2 in the feed, which come from lowering the *M*-module, enhance r-WGS reaction, leading to increased CO formation. In contrast, inclusion of CO in the feed is expected to promote CO and CO_2 hydrogenation reactions. Hence, investigating the performance of lower *M*-modules in the rest of industrial cases is recommended for future studies.

The *M*-module is defined by eqn (14) and shows the ratio between hydrogen and carbon in the feed. A value equal to 2 corresponds to the stoichiometric requirement of the system for a theoretical full conversion of CO and/or CO_2. Operating

at lower *M*-modules reduces the formation of both CO_2 and MeOH, thereby increasing the conversion to CO, whose recycling strategy might be more interesting. Like CO_2, increasing MeOH content is associated with higher energy requirements in the purification section. Separation of CO_2 is the most difficult step in the downstream DME purification due to the high affinity of the two components, and proximity and shape of their vapor–liquid equilibrium curves. In this context, the separation of CO_2 and DME can be performed very efficiently using the newly developed concept of stripping enhanced distillation (SED).[62] Additionally, as explained by Skorikova *et al.*,[22] MeOH must be separated from water in the final distillation column, since it exceeds the limit of ISO standard. Further reduction of the *M*-module could potentially eliminate the need for a MeOH separation column entirely, leading to both operational and capital savings. As discussed before, additional strategies to decrease carbon-to-methanol selectivity include reducing the CO content in the feed, increasing reactor temperature and lowering the feed flow rate. An example of substantial methanol content reduction in the product stream is illustrated in Fig. 6, where the overall carbon selectivity at two cycle durations (120 min and 180 min) at 35 bar is analysed for different *M*-modules for case 1. Operating at M = 1 results in MeOH selectivity of 0.15% and 0.18% for the 120 min and 180 min cycles, respectively. The productivity remains at operable levels of 1.6 kg h^{-1} and 2.2 kg h^{-1} for the M = 1 cases of 120 min and 180 min, respectively, with potential for further improvement by increasing pressure. The presence of CO in the product stream is an important factor to consider when optimising carbon selectivity to DME. As shown in Fig. 4a in the annex, CO will always be formed due to the interaction of the r-WGS.

2.2.3 Effect of feed flow. As mentioned, the flow rate used in all the aforementioned simulations is 20 Nm^3 h^{-1}, which is considered the maximum volumetric flow that can be supplied, by design, in the SEDMES pilot plant. In addition to flow composition, reducing the flow rate, and hence the gas hourly space velocity (GHSV), can also significantly impact the performance of the process, resulting in a longer residence time in the reactor. This longer contact time of reactants and catalyst allows for more extensive reaction, leading to higher conversion rates of carbon to DME. Additionally, as observed by van Kampen *et al.*,[1] the lower flow rate reduces water breakthrough and maintains the effectiveness of adsorption enhancement throughout the adsorption step. As depicted in Fig. 7a, at 25 bar operation of case 1, nominal flow (13.3 Nm^3 h^{-1}) results in a significant increase of DME selectivity when comparing maximum flow (20 Nm^3 h^{-1}), which aligns with the results of van Kampen *et al.*[1] and Tyraskis *et al.*[52] The maximum productivity of DME is 2.76 kg h^{-1}, achieved at 66% selectivity for maximum flow, whereas for nominal flow, it is 2.22 kg h^{-1} at 84% selectivity. The substantial increase in selectivity of nominal flow results in only 19.5% reduction of the productivity, despite reducing the reactants by 33.5%. These results indicate that the SEDMES process could operate under intermittent feed flow conditions caused by fluctuations of renewable electricity, without compromising overall performance. Future studies focusing on lower flows than the nominal and dynamic operation are recommended to thoroughly assess this capability.

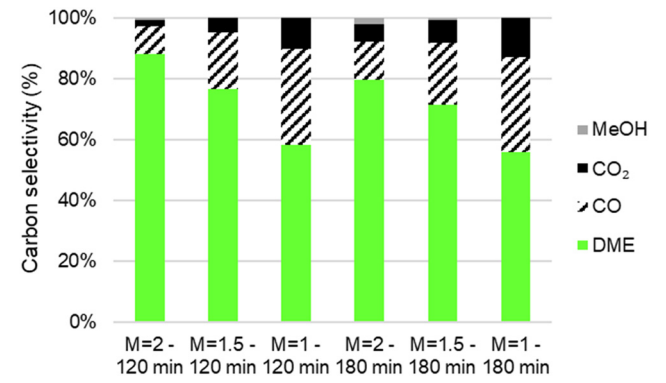

Fig. 6 Comparison of the performance of different *M*-modules for case 1 at 35 bar for 120 and 180 min cycle durations (35 bar).

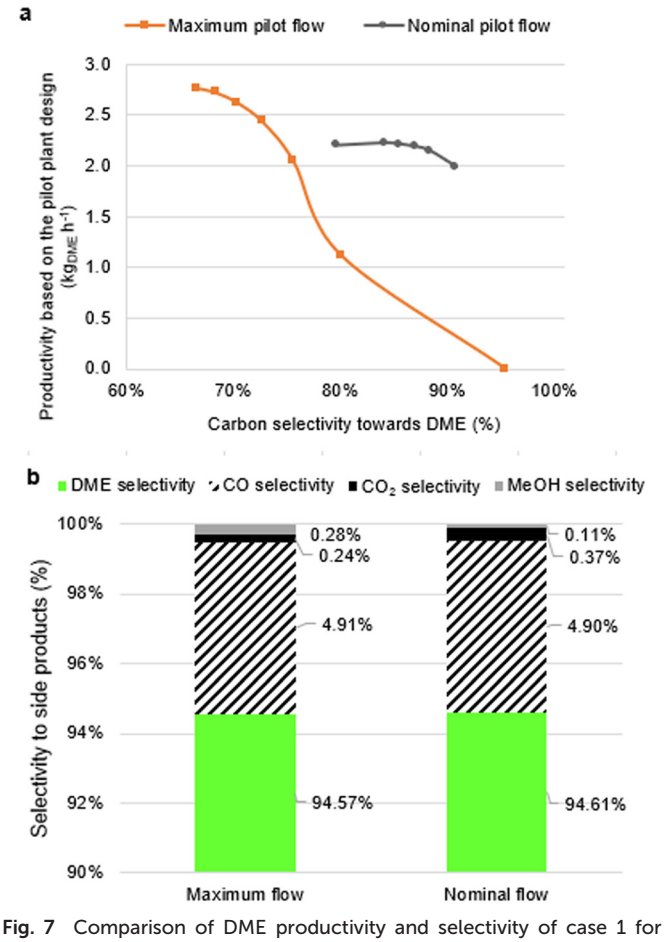

Fig. 7 Comparison of DME productivity and selectivity of case 1 for maximum and nominal flow rates (a) and carbon selectivity to by-products at similar carbon selectivity to DME (b). Pressure = 25 bar.

An additional effect that has not been analysed in previous studies is that the increased residence time favours methanol dehydration (eqn (4)) leading to improvement in DME selectivity and reduction of the amount in methanol in the product stream. In order to demonstrate this effect, two points with comparable DME selectivity at different flow rates (maximum and nominal) are analysed for case 1 at 30 bar operation, as shown in Fig. 7b. It is clear that the longer residence time of nominal flow promotes methanol dehydration, resulting in an end product of similar DME purity, but containing 40% lower amount of methanol.

2.2.4 Effect of temperature. Temperature can also play a role in the optimisation of the SEDMES process. As explained by J. van Kampen *et al.*,[21] despite the fact that the temperature for methanol dehydration is generally higher,[63] direct DME synthesis is often performed at temperatures of around 250 °C not only because methanol synthesis is considered to be the rate determining step in direct DME synthesis but also to prevent deactivation of the CZA catalyst at temperatures above 300 °C.[35,54,64–66] Therefore, the effect of the temperature in the DME productivity and *C*-selectivity towards DME is explained in Fig. 8a and b respectively, considering the temperature range 240–280 °C.

The results show that a moderate increase in the temperature can have a positive effect in the performance of SEMDES. Further increase of current simulations at 250 °C to 260 °C can increase both productivity and selectivity up to 6%, resulting in 3.84 kg h^{-1} productivity and 93% DME selectivity at 50 bar. However, when the temperature is higher than 260 °C, the performance of the process does not improve anymore which is a result of the compromise between the reaction rate and kinetic conversion. Between 260–280 °C, the DME productivity exhibited an insignificant decline of <2% at 35 and 50 bar and a more noticeable drop of 7% at 20 bar (Fig. 8a). Selectivity to DME decreased more visibly, dropping by 5% at 35 and 50 bar and 9% at 25 bar. Higher temperatures increase the reaction rate but reduce equilibrium conversion, and this balance may shift slightly under varying pressures. Additionally, since DME synthesis benefits from the increase in pressure, at low pressure, the competition with the r-WGS plays a more significant role promoting more significant changes in the DME productivity in the low pressure range. Additionally, the higher productivity and selectivity drop at lower pressures and high temperatures aligns with the results of Le J. *et al.* who showed that increasing the pressure favours the molar decreasing reaction of CO_2 hydrogenation to methanol.[2] In the current study, for every pressure studied, operation at 260 °C provided the best performance. The results align with the study of van Kampen *et al.*, where the optimum DME yield was achieved between 250 and 275 °C.[1] An additional point that should be taken into account when deciding an optimum temperature is the influence of temperature fluctuations during the reaction process considering that this type of system is exothermic. A previous study showed that the model is able to capture the behaviour of the temperature

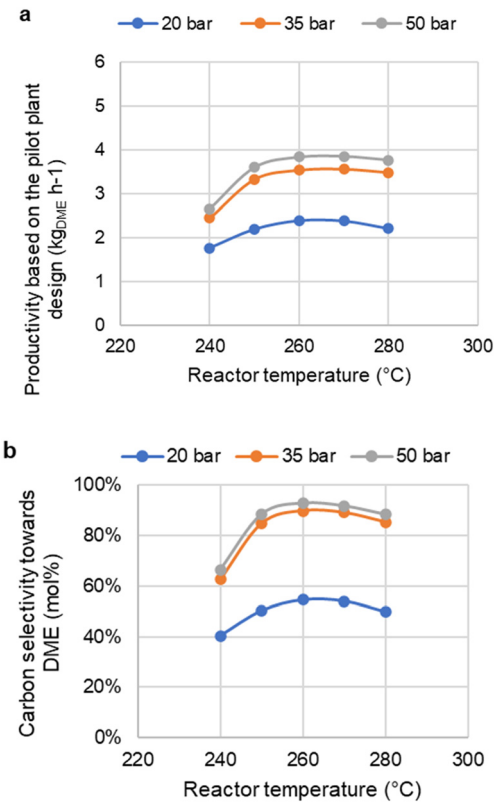

Fig. 8 Effect of reactor temperature on the carbon selectivity towards DME (a) and pilot design DME productivity (b).

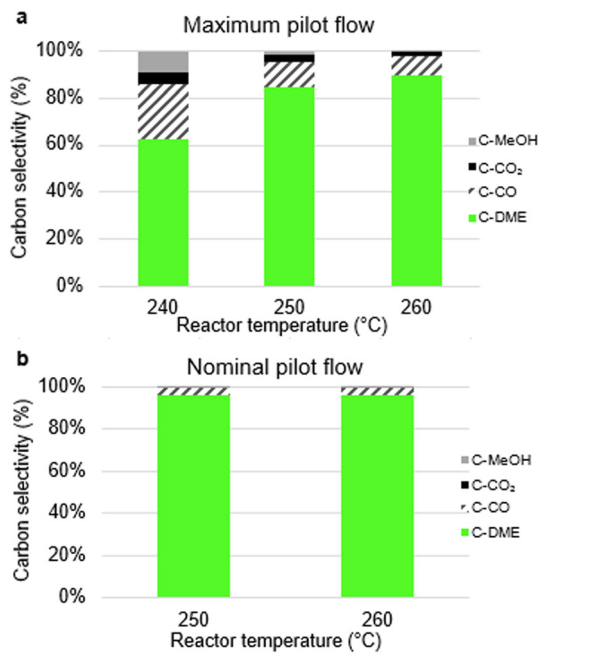

Fig. 9 Bar chart showing the carbon selectivity to DME and by-products for different temperature levels for case 1 at 35 bars. (a) shows a simulation at the maximum pilot design flow rate and (b) a simulation at the nominal pilot design flow rate.

profile across the reactor length showing a maximum ΔT of 20 °C.[12] Therefore, the selected 260 °C optimum also ensures that the maximum temperature of 300 °C is not reached at any point of the column preventing catalyst deactivation due to temperature fluctuations during the reaction process.

Thus, since the feed flow has an impact in the selectivity, the effect of the temperature was also compared for two feed flows, maximum (20 $Nm^3\ h^{-1}$) and nominal (13.3 $Nm^3\ h^{-1}$) as reflected in Fig. 9a and b, respectively. When the SEDMES pilot plant design is operated with a nominal feed flow, the effect of the temperature on productivity and selectivity to DME is minimal. Notice that, in the case of nominal feed flow MeOH and CO_2 impurities are absent at 250 °C, and the carbon that is not converted into DME is mostly present, only, as CO which could be a result of the r-WGS reaction. On the contrary, at the maximum feed flow MeOH and CO_2 by-products are present at higher concentrations and they are minimised with the increase of temperature up to 260 °C.

It is concluded that increasing the operating temperature above 250 °C, up to 260 °C, can be beneficial in cases of low DME selectivity. However, increasing the temperature when by-product formation is already minimised will not enhance DME selectivity or productivity. It is important to note that while higher temperatures increase the catalyst activity – as long as it does not deactivate – they also limit the adsorption capacity of the system.[1] Hence, the optimum operating temperature also depends on the water hold-up and may vary depending on other parameters. Furthermore, as reported by Jia *et al.*, the equilibrium conversion of CO declines gradually with an increase in temperature because all of the involved reactions – methanol synthesis reactions from CO hydrogenation, the WGS reaction, and the methanol dehydration reactions – are exothermic reactions.[2] On the other hand the CO_2 hydrogenation process is less exothermic than CO hydrogenation and also involves r-WGS which is an endothermic reaction. Hence, inclusion of CO in the feed is expected to worsen the positive results of increasing operating temperature above 250 °C. Further research of the phenomenon for case 2, 3 and 4 is proposed for future development.

3 Conclusions

In this study, four industrial use cases of SEDMES process application were analysed, featuring progressively higher CO/CO_2 ratios in the feed. A clear relationship between the CO/CO_2 ratio in the feed and the SEDMES performance was established. Increasing the CO content resulted in an almost linear increase in DME productivity. Case 4 (indirect biomass gasification with higher CO content) achieved a productivity of 4.67 kg h^{-1} at 50 bars – an improvement of 32% compared to the CO-free case 1 (natural gas cleaning), which reached 3.53 kg h^{-1}. Although DME selectivity near the maximum productivity points was not significantly influenced, minor improvements were observed with increased CO content in the feed, such as a 1.7% increase for case 4. Despite these advantages, higher CO content consistently led to higher CO_2 levels in the product, which are challenging to recycle and require additional energy for purification. On the other hand, selectivity toward MeOH, which also increases purification requirements, was slightly reduced in higher-CO cases (indirect gasification and steel off-gases), particularly at 50 bars. In the cases with more CO content in the feed (indirect biomass gasification and steel off-gas), SEDMES performance is enhanced in terms of DME selectivity and productivity while requiring up to 30% less H_2 in the feed, improving the overall efficiency of the process.

The *M*-module influenced carbon selectivity toward by-products. Lowering the *M*-module led to increased CO selectivity and reduced CO_2 selectivity at comparable DME selectivity levels. Additionally, methanol selectivity was further reduced, potentially eliminating the need for a methanol separation column in downstream processing. Water hold-up was the main driver for both the CO/CO_2 ratio and *M*-module effects on by-product formation. The study also demonstrated that the SEDMES process could operate effectively under intermittent feed flow conditions caused by fluctuations in renewable electricity supply. A 66% reduction in feed flow for case 1 (natural gas cleaning) at 25 bars increased DME selectivity by 18%, without compromising overall performance. This reduction also lowered the methanol content in the product by 60%. Finally, an increase in operating temperature from 250 °C to 260 °C enhanced system performance for cases with unconverted carbon, improving both DME productivity and carbon selectivity up to 6%.

The SEDMES design study has thus shown the inherent flexibility in the process to adapt to various feed conditions and to allow for optimisation towards various design targets, while maintaining an attractive high DME yield. The resilience of the SEDMES process under lower feed flow conditions potentially caused by renewable electricity fluctuations has to be demonstrated experimentally. Additionally, further studies should be focused on minimising the residual CO content in the system to improve the single-pass carbon conversion. An interesting research line for this topic would be testing new catalysts that inhibit or reduce the formation of CO *via* the r-WGS reaction.

4 Methodology

To evaluate the flexibility of the SEDMES process, different industrial use cases are compared in this work. The SEDMES results are obtained by modelling the process using a one-dimensional pseudo-homogeneous dynamic reactor model developed in a previous study.[1] For the description of the fluid flow and mass transfer, the 1D non-steady differential mass and momentum balances are solved. The total mass, momentum, component and overall energy balances are collected in Table 2. Reaction kinetics were determined for the catalysts by fitting the parameters in the models of Graaf *et al.* (1988) and Berčič *et al.* (1992) for the methanol

Table 2 Reactor model equations

Continuity/overall mass balance	$\frac{\partial \rho}{\partial t} = -\frac{\partial \rho v}{\partial z} - \frac{1-\varepsilon_b}{\varepsilon_b} a_p \sum M_i N_i$	(5)
Momentum balance	$\frac{\partial \rho v}{\partial t} = -\frac{\partial \rho v^2}{\partial z} - \frac{\partial P}{\partial z} - G\frac{\rho \lvert u \rvert u}{d_p}$	(6)
Species mass balance	$\frac{\partial \rho \omega_i}{\partial t} = -\frac{\partial \rho v \omega_i}{\partial z} + \frac{\partial}{\partial z}\left(D_z \rho \frac{\partial \omega_i}{\partial z}\right) - \frac{1-\varepsilon_b}{\varepsilon_b} a_p M_i N_i$	(7)
Overall energy balance	$\left(\varepsilon_b \rho \mathrm{Cp} + (1-\varepsilon_b)\rho_p \mathrm{Cp}_p\right)\frac{\partial T}{\partial t} = -\rho \mathrm{Cp} u \frac{\partial T}{\partial z} + \frac{\partial}{\partial z}\left(\lambda \frac{\partial T}{\partial z}\right) + \frac{4U(T_w - T)}{d_r} + (1-\varepsilon_b)\rho_p\left(\sum -\Delta H_{r,i} r_i + \sum -\Delta H_{ads,i}\frac{\partial \overline{q_i}}{\partial t}\right)$	(8)
Equation of state	$\mathrm{PM} = \rho R T$	(9)

synthesis and methanol dehydration, respectively, and are shown in Table 3.[67–69] The steam adsorption isotherm of the LTA zeolite adsorbent was determined under the high pressure and temperature working conditions of the SEDMES process. A Sips isotherm best describes the experimental data, in accordance with the available literature at lower temperature and pressure conditions.[70,71] The resulting set of partial differential equations for the column was solved by an in-house developed code using the method of lines, and MATLAB (release 2023b) built-in variable order solver 'ode15s' that was able to deal with the stiffness of the system due to sharp concentration gradients appearing in the convection–reaction–adsorption system. Using an in-house developed routine, the column model was used to simulate individually the consecutive steps of the SEDMES cycle: adsorption (ADS), blowdown (BD), purge (P), and re-pressurisation (REP), discussed below. For each of the steps, the final state of the column in the preceding step was taken as the initial state of the column. Specifically for the momentum balance, the code was stabilised by a smoothed transition (0.1 s) from the preceding pressure-flow distribution to the new state. With the routine, the discontinuous inlet and outlet streams were added to arrive at the predicted behaviour of the ensemble of three columns. Full details of the different aspects of the model can be found in a previous study.[1]

The SEDMES model is based on a complex set of equations with numerous parameter estimates which have a pronounced impact on the model results. Model validation has been done previously in order to confirm the accuracy. Reaction kinetics were evaluated on the basis of more critical breakthrough experiments,[1] and the kinetic parameters for these equations were refitted based on a dedicated kinetic study.[21] Specifically for the adsorption isotherm and kinetics for steam adsorption on zeolite 3A, systematic experiments have been performed under non-reactive conditions, which led to the derivation of a validated adsorption isotherm and linear driving force mass transfer relation valid under SEDMES conditions.[72] Finally, experimental validation of system performance is currently underway in the 3-column pilot reactor.

The cases analysed in this study are based on three industrial use cases: natural gas cleaning, indirect biomass gasification and steel off-gas, and were chosen to represent a gradual increase in the CO/CO_2 ratio, ranging from 0 to 3.24. The cases are:

- Case 1: upstream natural gas processing with preliminary CO_2 capture.
- Case 2: indirect biomass gasification product 1 (CO_2-rich syngas).
- Case 3: steel off-gas without preliminary CO_2 capture.

Table 3 Reaction rate equations for methanol synthesis and methanol dehydration. Reaction conditions for the methanol synthesis are P = 15–51 bar and T = 180–280 °C using a commercial CuZnAl catalyst. Reaction conditions for the methanol dehydration are atmospheric pressure in a temperature range of 290–360 °C using a commercial γ-Al_2O_3 catalyst

Methanol synthesis from CO[68]	$r_{CH_3OH,1} = \frac{k_1 K_{CO}\left[\varphi_{CO}\varphi_{H_2}^{3/2} - \varphi_{CH_3OH}/\left(\varphi_{H_2}^{1/2} K_{p1}\right)\right]}{\left(1 + K_{CO}\varphi_{CO} + K_{CO_2}\varphi_{CO_2}\right)\left[\varphi_{H_2}^{1/2} + \left(K_{H_2O}/K_{H_2}^{1/2}\right)\varphi_{H_2O}\right]}$	(10)
Water gas shift[68]	$r_{CO} = \frac{k_2 K_{CO_2}\left[\varphi_{CO_2}\varphi_{H_2} - \varphi_{H_2O}\varphi_{CO}/K_{p2}\right]}{\left(1 + K_{CO}\varphi_{CO} + K_{CO_2}\varphi_{CO_2}\right)\left[\varphi_{H_2}^{1/2} + \left(K_{H_2O}/K_{H_2}^{1/2}\right)\varphi_{H_2O}\right]}$	(11)
Methanol synthesis from CO_2 (ref. 68)	$r_{CH_3OH,2} = \frac{k_3 K_{CO_2}\left[\varphi_{CO_2}\varphi_{H_2}^{3/2} - \varphi_{CH_3OH}\varphi_{H_2O}/\left(\varphi_{H_2}^{3/2} K_{p3}\right)\right]}{\left(1 + K_{CO}\varphi_{CO} + K_{CO_2}\varphi_{CO_2}\right)\left[\varphi_{H_2}^{1/2} + \left(K_{H_2O}/K_{H_2}^{1/2}\right)\varphi_{H_2O}\right]}$	(12)
Methanol dehydration[69]	$r_{DME} = \frac{k_4 K_{CH_3OH}^2\left[C_{CH_3OH}^2 - C_{H_2O}C_{DME}/K_{p4}\right]}{\left[1 + 2\left(K_{CH_3OH}C_{CH_3OH}\right)^{1/2} + K_{H_2O}C_{H_2O}\right]^4}$	(13)

Table 4 Feed composition of the four industrial cases

Wt%	H_2	CO	CO_2	H_2O	N_2	CH_4
Case 1	12.1	—	87.9	—	—	—
Case 2	11.6	12.4	71.0	1.5	2.3	1.3
Case 3	11.8	42.3	41.6	0.8	2.2	1.2
Case 4	11.9	63.2	19.5	1.6	2.5	1.4
Case 1-imp	11.5	—	83.5	1.3	2.4	1.3

- Case 4: indirect biomass gasification product 2 (CO-rich syngas).

The levels of inert gases and water are nearly identical in each case, ensuring that these factors do not significantly impact the assessment. Four cases are studied whose composition is shown in Table 4. Cases 2, 3, and 4 exhibit similar levels of inert gases and water content, ranging from 4.2 to 5.5 wt%. In contrast, case 1 has no impurities in the feed stream, which is expected to enhance its performance. This study seeks to compare real industrial cases; however, to allow a fair comparison of the effect of the CO/CO_2 ratio on performance, it is crucial to account for the influence of small amounts of inert gases.[73] Therefore, case 1 was also simulated with the inclusion of 5 wt% inerts, with the precise composition detailed in Table 4, case1-imp. While the actual industrial case 1 is utilised throughout the paper, the adjusted version with impurities is referenced where appropriate to highlight the subtle impact of the absence of inert gases. The operation conditions are 250 °C, P in the range 20–50 bar and cycle times 75–330 min. These conditions are considered representative in view of the previous experimental results.[16–21] The Pareto plots are built scanning different cycle times (the lower the carbon selectivity the higher the cycle time).

SEDMES is a reactive adsorption process in which steam is removed *in situ* by an adsorbent and as a typical pressure swing adsorption (PSA) system, it is operated in cycles. Each cycle has four consecutive steps: adsorption (ADS) is the step in which DME is produced with *in situ* water removal under the selected pressure; blowdown (BD) is the depressurisation of the system in order to prepare the system for the pressure swing regeneration; purge (P) is the step in which the water adsorbent is regenerated using H_2 as purge gas at ambient pressure and finally, re-pressurisation (REP) is when the column is re-pressurised in order to be ready for the next ADS step (Fig. 10a). H_2 is used for the re-pressurisation step unless otherwise specified. In this work, the largest dedicated SEDMES installation built at TNO Petten, The Netherlands, is used as reference for the cycle design (Fig. 10b). Note that the pilot plant has been used here as a reference in terms of reactor size and operation window. Future work will present operational data from the pilot plant, which are currently being collected, to allow for experimental validation of the conclusions in this work. The SEDMES pilot plant is equipped with three reactor columns, working as a shell and tube heat exchanger reactor. Inside each reactor there are 19 tubes of 7.6 m height and 36.6 mm internal diameter. Copper-based methanol synthesis and gamma alumina dehydration catalysts are present in the reactors, as well as a zeolite 3A for *in situ* water removal.[72,74] The catalyst fraction is 0.2. Heat management, consisting of cooling the heat of

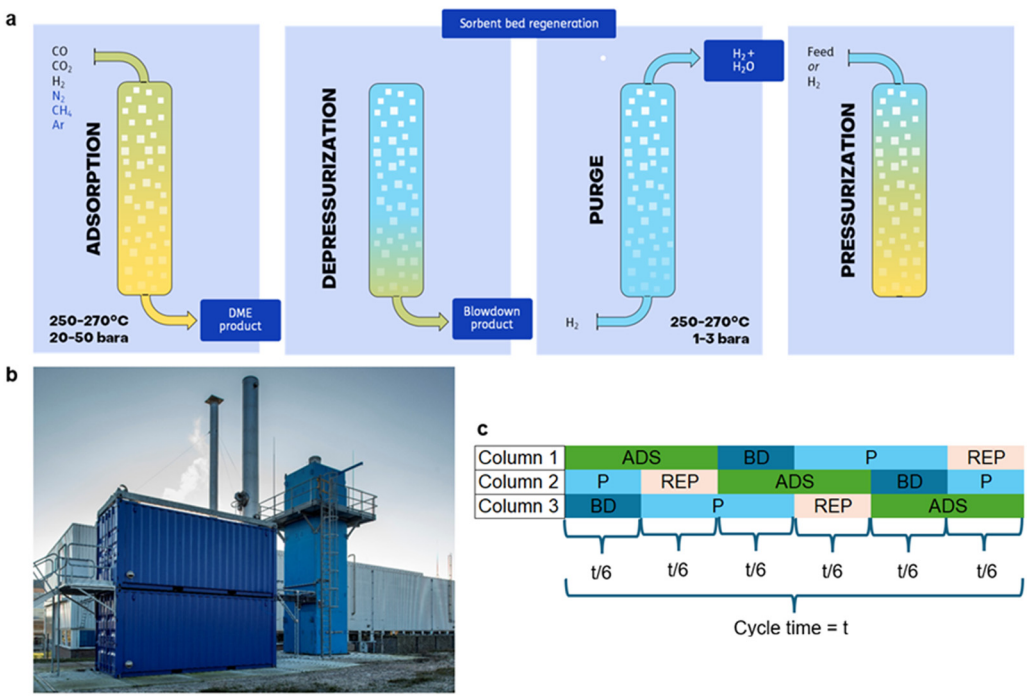

Fig. 10 Steps of the SEDMES process operating as a pressure swing regeneration unit – PSA (a); SEDMES pilot plant at TNO, Petten, The Netherlands, designed to produce 3 kg_{DME} h^{-1} (b) and cycle design operating in the pilot plant (c).

reaction and the heat of adsorption, and supplying the heat for the endothermic water desorption, is done by thermal oil in the reactors shell.[8] The three reactors are producing DME continuously by going through the various steps according to the cycle design shown in Fig. 10c.

In all the scenarios unless otherwise specified, the *M*-module (eqn (14)) is equal to 2 and maximum feasible flow of the pilot plant has been assumed for the adsorption, purge and re-pressurisation steps (20, 25 and 34 $Nm^3\ h^{-1}$, respectively). The influence of the CO/CO_2 ratio was previously examined by Guffanti *et al.*,[12] though without specific optimisation of the cycle design. In this study, we identify the optimal operating conditions for each case and further investigate the potential of various feed compositions. In order to find the region of optimal operation for the different case studies and pressures, different cycle times were simulated for six different pressures (20, 25, 30, 35, 40 and 50 bar), and the temperature has been fixed to 250 °C. The performance was evaluated by analysing the Pareto plots showing the DME productivity and carbon selectivity curves at the different operating pressures. This was achieved by changing the duration of each step of the cycle while keeping the ratio of step time over total cycle time constant to ensure continuous operation.

$$M\text{-module} = \frac{H_2\ (\text{mol\%}) - CO_2\ (\text{mol\%})}{CO\ (\text{mol\%}) + CO_2\ (\text{mol\%})} \quad (14)$$

Case 1 has been subjected to the highest number of simulations and it has been primarily used to evaluate the process's performance and draw conclusions about its efficiency in a previous study.[52] The effects of operating pressure, cycle duration, amount of inert gases, tube geometry and feed flow rate were analysed and it was shown that an increased operating pressure led to increased carbon selectivity and productivity at the expense of a higher DME loss in the pressure swing operation. In the current study, its performance was compared to that of other cases, each featuring different feed compositions, to determine the effect of CO/CO_2 concentrations in the performance and operation of the SEDMES process. Furthermore, case 1 was utilised to gain further insights into the effect of feed composition by varying the *M*-module, and examine the impact of operating temperature. The main key performance indicators (KPIs) in this work are the SEDMES pilot plant DME productivity and the carbon selectivity towards DME (S(DME)) and other products (i) such as MeOH, CO_2 or CO. These KPIs are calculated using eqn (15)–(17), respectively. The carbon selectivity is calculated as molar concentration-based selectivity for each of the carbon containing species $y(i)$.

$$\text{DME productivity}\ \left(kg_{DME}\ h^{-1}\right) = \frac{\text{DME production (kg)}}{\text{Cycle time (h)}} \quad (15)$$

$$S(\text{DME}) = \frac{2y(\text{DME})}{y(\text{CO}) + y(CO_2) + y(\text{MeOH}) + 2y(\text{DME})} \quad (16)$$

$$S(i) = \frac{y(i)}{y(\text{CO}) + y(CO_2) + y(\text{MeOH}) + 2y(\text{DME})} \quad (17)$$

$$\text{Carbon conversion to DME (\%)} = \frac{n_{DME,out}}{n_{CO_2,in}} \cdot 100 \quad (18)$$

Nomenclature

ΔH_r^0	Standard enthalpy of reaction
a_p	Particle interface are ($m^2\ m^{-3}$)
c_i	Concentration of component i (mol m^{-3})
Cp	Gas thermal conductivity (J $kg^{-1}\ K^{-1}$)
Cp_p	Particle thermal conductivity (J $kg^{-1}\ K^{-1}$)
d_c	Crystal diameter (m)
d_p	Particle diameter (m)
D_c	Micropore diffusion coefficient ($m^2\ s^{-1}$)
D_k	Knudsen diffusion coefficient ($m^2\ s^{-1}$)
D_m	Molecular diffusion coefficient ($m^2\ s^{-1}$)
D_p	Macropore diffusion coefficient ($m^2\ s^{-1}$)
D_z	Axial dispersion coefficient ($m^2\ s^{-1}$)
G	Ergun constant (—)
ΔH_{ads}	Adsorption enthalpy (J mol^{-1})
$\Delta H_{r,i}$	Reaction enthalpy (J mol^{-1})
k	Reaction rate constant (mol $s^{-1}\ kg^{-1}\ bar^{-1}$) or (kmol $kg^{-1}\ h^{-1}$)
K_i	Adsorption equilibrium constant of component i (bar^{-1}) or ($m^3\ kmol^{-3}$)
K_p	Equilibrium constant (based on partial pressure) (—)
M_i	Molecular weight of component i (kg mol^{-1})
N_i	Molar flux of component i (mol $m^{-2}\ s^{-1}$)
P	Reactor pressure (bara)
P_i	Partial pressure of component i (bara)
q_i	Adsorbent loading (mol kg^{-1})
r_i	Reaction rate of component i (mol $m^{-3}\ s^{-1}$) or (mol $kg^{-1}\ s^{-1}$) or (kmol $kg^{-1}\ h^{-1}$)
R	Ideal gas constant (J $mol^{-1}\ K^{-1}$)
t	Time (s)
T	Temperature (K)
u	Superficial gas velocity (m s^{-1})
U	Overall heat transfer coefficient (W $m^{-2}\ K^{-1}$)
v	Interstitial gas velocity (m s^{-1})
z	Axial coordinate (m)

Greek letters

ε_b	Bed voidage (—)
ε_p	Particle porosity (—)
λ	Axial thermal conductivity (W $m^{-1}\ K^{-1}$)
ρ	Density (kg m^{-3})
ρ_p	Particle density (kg m^{-3})
φ_i	Partial fugacity of component i (bara)
ω_i	Weight fraction of component i (—)

Data availability

The data supporting this article have been included in the main text and as part of the ESI.† Any further details will be available upon request.

Author contributions

IT: writing – original draft, writing – review and editing, visualization. AC: writing – original draft, writing – review and editing, visualization. GS: writing – review and editing, validation. SS: writing – review and editing, validation. JB: writing – review and editing, validation.

Conflicts of interest

The authors declare no conflict of interest.

Acknowledgements

The work in this publication was performed with a subsidy from the Ministry of Economic Affairs and Climate and the Ministry of Agriculture, Nature and Food Quality, National EZK and LNV subsidy schemes, Top Sector Energy implemented by the Netherlands Enterprise Agency (RVO) (MOOI422003 and TIND121006).

References

1 V. Kampen, J. Boon, J. Vente and M. Van Sint Annaland, Sorption enhanced dimethyl ether synthesis for high efficiency carbon conversion: Modelling and cycle design, *J. CO2 Util.*, 2020, **37**, 295–308.
2 J. Le, N. Yin and Y. Fong, Catalytic conversion of CO_2 to dimethyl ether: A review of recent advances in catalysts and water selective layer, *J. Ind. Eng. Chem.*, 2024, **140**, 88–102.
3 R. P. Verbeek, A. van Doorn, M. van Walwijk and T. Wegtransportmiddelen, Global assessment of dimethyl-ether as an automotive fuel, *TNO Rep.*, 1996, p. 75.
4 C. Arcoumanis, C. Bae, R. Crookes and E. Kinoshita, The potential of di-methyl ether (DME) as an alternative fuel for compression-ignition engines: A review, *Fuel*, 2008, **87**, 1014–1030.
5 T. H. Fleisch, A. Basu, M. J. Gradassi and J. G. Masin, Dimethyl ether: A fuel for the 21st century, in *Natural Gas Conversion IV*, 1997, vol. 107, pp. 117–125.
6 Y. Putrasari and O. Lim, Dimethyl ether as the next generation fuel to control nitrogen oxides and particulate matter emissions from internal combustion engines: A review, *ACS Omega*, 2022, **7**, 32–37.
7 D. Cocco, V. Tola and G. Cau, Performance evaluation of chemically recuperated gas turbine (CRGT) power plants fuelled by di-methyl-ether (DME), *Energy*, 2006, **31**, 1446–1458.
8 C. Peinado, D. Liuzzi, S. Sluijter, G. Skorikova, J. Boon, S. Guffanti, G. Groppi and S. Rojas, Review and perspective : Next generation DME synthesis technologies for the energy transition, *Chem. Eng. J.*, 2024, **479**, 147494.
9 Z. Azizi, M. Rezaeimanesh, T. Tohidian and M. R. Rahimpour, Dimethyl ether: A review of technologies and production challenges, *Chem. Eng. Process.*, 2014, **82**, 150–172.
10 K. Saravanan, H. Ham, N. Tsubaki and J. W. Bae, Recent progress for direct synthesis of dimethyl ether from syngas on the heterogeneous bifunctional hybrid catalysts, *Appl. Catal., B*, 2017, **217**, 494–522.
11 F. Dadgar, R. Myrstad, P. Pfeifer, A. Holmen and H. J. Venvik, Direct dimethyl ether synthesis from synthesis gas: The influence of methanol dehydration on methanol synthesis reaction, *Catal. Today*, 2016, **270**, 76–84.
12 S. Guffanti, C. G. Visconti, J. van Kampen, J. Boon and G. Groppi, Reactor modelling and design for sorption enhanced dimethyl ether synthesis, *Chem. Eng. J.*, 2021, **404**, 126573.
13 H. Li, S. Ren, S. Zhang, S. Padinjarekutt, B. Sengupta, X. Liang, S. Li and M. Yu, The high-yield direct synthesis of dimethyl ether from CO_2 and H_2 in a dry reaction environment, *J. Mater. Chem. A*, 2021, **9**, 2678–2682.
14 Q. Dong, W. L. Xu, X. Fan and H. Li, Prototype catalytic membrane reactor for dimethyl ether synthesis via CO_2 hydrogenation, *Ind. Eng. Chem. Res.*, 2022, **61**, 14656–14663.
15 I. Iliuta, M. C. Iliuta and F. Larachi, Sorption-enhanced dimethyl ether synthesis-Multiscale reactor modeling, *Chem. Eng. Sci.*, 2011, **66**, 2241–2251.
16 J. Boon and F. P. F. Van Berkel, Separation enhanced dimethyl ether synthesis, *Fifth Int. Conf.*, 2017, pp. 20–22.
17 D. Liuzzi, C. Peinado, M. A. Pena, J. Van Kampen, J. Boon and S. Rojas, Increasing dimethyl ether production from biomass-derived syngas via sorption enhanced dimethyl ether synthesis, *Sustainable Energy Fuels*, 2020, **4**, 5674–5681.
18 N. S. Altinsoy and A. K. Avci, Sorption enhanced DME synthesis by one-step CO_2 hydrogenation, *Chem. Eng. Process.*, 2024, **203**, 109874.
19 J. Van Kampen, J. Boon, F. P. F. Berkel, H. A. J. van Dijk, F. J. Vente and M. van Sint Annaland, Regeneration conditions as the key to sorption enhanced dimethyl ether synthesis, *25th Int. Conf. Chem. React. Eng.*, 2018, vol. 1, pp. 3–4.
20 J. Van Kampen, S. Booneveld, J. Boon, J. Vente and M. Van Sint Annaland, Experimental validation of pressure swing regeneration for faster cycling in sorption enhanced dimethyl ether synthesis, *Chem. Commun.*, 2020, **56**, 13540–13542.
21 J. Van Kampen, J. Boon, J. Vente and M. Van Sint Annaland, Sorption enhanced dimethyl ether synthesis under industrially relevant conditions: Experimental validation of pressure swing regeneration, *React. Chem. Eng.*, 2021, **6**, 244–257.
22 G. Skorikova, M. Saric, S. N. Sluijter, J. Van Kampen, C. Sánchez and J. Voon, The techno-economic benefit of sorption enhancement: Evaluation of sorption-enhanced

dimethyl ether synthesis for CO_2 utilization, *Front. Chem. Eng.*, 2020, **2**, 1–11.

23 G. A. Olah, A. Goeppert and G. K. S. Prakash, Chemical recycling of carbon dioxide to methanol and dimethyl ether: From greenhouse gas to renewable, environmentally carbon neutral fuels and synthetic hydrocarbons, *J. Org. Chem.*, 2009, **74**, 487–498.

24 A. Livescu, R. Navar, J. R. Mangalindan, F. Mahnaz, Y. Ge, M. Shetty and X. Yang, Catalysts for clean energy: A review on current progress for the catalyzed recycling of CO_2 into dimethyl ether, *Top. Catal.*, 2024, DOI: **10.1007/s11244-024-01913-z**.

25 E. T. C. Vogt and B. M. Weckhuysen, The refinery of the future, *Nature*, 2024, **629**, 295–306.

26 L. Deng and T. A. Adams, Comparison of steel manufacturing off-gas utilization methods via life cycle analysis, *J. Cleaner Prod.*, 2020, **277**, 123568.

27 L. Deng and T. A. Adams, Techno-economic analysis of coke oven gas and blast furnace gas to methanol process with carbon dioxide capture and utilization, *Energy Convers. Manage.*, 2020, **204**, 112315.

28 M. h. Gong, Q. Yi, Y. Huang, G.-S. Wu, Y.-H. Hao, J. Feng and W.-Y. Li, Coke oven gas to methanol process integrated with CO_2 recycle for high energy efficiency, economic benefits and low emissions, *Energy Convers. Manage.*, 2017, **133**, 318–331.

29 S. Kim and J. Kim, The optimal carbon and hydrogen balance for methanol production from coke oven gas and Linz-Donawitz gas: Process development and techno-economic analysis, *Fuel*, 2020, **266**, 117093.

30 J. Lundgren, T. Ekbom, C. Hulteberg, M. Larsson, C.-E. Grip, L. Nilsson and P. Tuna, Methanol production from steel-work off-gases and biomass based synthesis gas, *Appl. Energy*, 2013, **112**, 431–439.

31 S. Shin, J. K. Lee and I. B. Lee, Development and techno-economic study of methanol production from coke-oven gas blended with Linz Donawitz gas, *Energy*, 2020, **200**, 117506.

32 H. Park, Y. Woo, H. S. Jung, G. Kim, J. W. Bae and M. J. Park, Development of dimethyl ether synthesis processes using by-product gas from a steel-making plant: Single-vs. two-step processes, *J. Cleaner Prod.*, 2021, **326**, 129367.

33 M. Jeon, S. Jeon, J. Yi and M. Park, Analysis of the techno-economics and CO_2 emissions of DME production using by-product gases in the steel industries, *J. Cleaner Prod.*, 2025, **492**, 144893.

34 C2FUEL - Carbon captured fuel and energy carriers for an intensified steel off-gases based electricity generation in a smarter industrial ecosystem, 2020, **https://cordis.europa.eu/project/id/838014**.

35 V. M. Lebarbier, A. D. Robert, L. Kovarik, J. A. Lizarazo, D. L. King and D. R. Palo, Synthesis of methanol and dimethyl ether from syngas over $Pd/ZnO/Al_2O_3$ catalysts, *Catal. Sci. Technol.*, 2012, **2**, 2116–2127.

36 R. Kofler, N. Campion, M. Hillestad, W. Meesenburg and L. R. Clausen, Techno-economic analysis of dimethyl ether production from different biomass resources and off-grid renewable electricity, *Energy Fuels*, 2024, **38**, 8777–8803.

37 P. C. Moura, M. A. de Araujo Filho, H. G. D. Villardi, R. M. Cavalcante and A. F. Young, Process simulation and economic evaluation of an integrated production plant for methanol, acetic acid and DME synthesis via sugarcane bagasse gasification, *Energy Convers. Manage.*, 2023, **286**, 117051.

38 K. Im-orb and P. Piroonlerkgul, Sustainability analysis of the bio-dimethyl ether (bio-DME) production via integrated biomass gasification and direct DME synthesis process, *Renewable Energy*, 2023, **208**, 324–330.

39 J. Zhang, Y. Wang, Y. Zhang, Q. Wu, L. Xin, Y. Zhou, K. Yin, Y. Wang, X. Li and P. Cui, A novel power, DME, and ammonia polygeneration system using Aspen plus based on the integration of biomass gasification and syngas chemical looping, *Energy Convers. Manage.*, 2024, **299**, 117808.

40 A. Giuliano and E. Catizzone, Modelling and environmental aspects of direct or indirect dimethyl ether synthesis using digestate as feedstock, *Math. Model. Eng. Probl.*, 2021, **8**, 780–786.

41 M. Fedeli, F. Negri, A. Bornazzini, L. Montastruc, F. Manenti and A. A. Kiss, Process design and downstream optimization of the direct synthesis route for cleaner production of dimethyl ether from biogas, *J. Cleaner Prod.*, 2024, **443**, 141060.

42 L. P. Merkouri, H. Ahmet, T. Ramirez Reina and M. S. Duyar, The direct synthesis of dimethyl ether (DME) from landfill gas: A techno-economic investigation, *Fuel*, 2022, **319**, 123741.

43 M. Fedeli, F. Negri and F. Manenti, Biogas to advanced biofuels: Techno-economic analysis of one-step dimethyl ether synthesis, *J. Cleaner Prod.*, 2022, **376**, 134076.

44 M. E. G. Ribeiro Domingos, D. Flórez-Orrego, M. Teles dos Santos, S. de Oliveira and F. Maréchal, Techno-economic and environmental analysis of methanol and dimethyl ether production from syngas in a kraft pulp process, *Comput. Chem. Eng.*, 2022, **163**, 107810.

45 M. E. Moghaddam, N. Dahmen, U. Santo and J. Sauer, Gasoline synthesis from biomass-derived syngas comparing different methanol and dimethyl ether pathways by process simulation, based on the bioliq process, *Energy Fuels*, 2024, **38**, 4229–4243.

46 M. Pozzo, A. Lanzini and M. Santarelli, Enhanced biomass-to-liquid (BTL) conversion process through high temperature co-electrolysis in a solid oxide electrolysis cell (SOEC), *Fuel*, 2015, **145**, 39–49.

47 F. M. Baena-Moreno, M. Gonzalez-Castaño, H. Arellano-García and T. R. Reina, Exploring profitability of bioeconomy paths: Dimethyl ether from biogas as case study, *Energy*, 2021, **225**, 120230.

48 W. Xu, L. Yang, Z. Niu, S. Wang, Y. Wang, Z. Zhu and P. Cui, Thermodynamic and economic analysis of a novel DME-power polygeneration system based on the integration of biomass gasification and alkaline electrolysis of water for hydrogen production, *Energy*, 2025, **314**, 134185.

49 A. M. Parvez, S. Hafner, M. Hornberger, M. Schmid and G. Scheffknecht, Sorption enhanced gasification (SEG) of

biomass for tailored syngas production with in-situ CO_2 capture: Current status, process scale-up experiences and outlook, *Renewable Sustainable Energy Rev.*, 2021, **141**, 110756.

50 I. Martínez and M. C. Romano, Flexible sorption enhanced gasification (SEG) of biomass for the production of synthetic natural gas (SNG) and liquid biofuels: Process assessment of stand-alone and power-to-gas plant schemes for SNG production, *Energy*, 2016, **113**, 615–630.

51 J. Boon, Sorption-enhanced reactions as enablers for CO_2 capture and utilisation, *Curr. Opin. Chem. Eng.*, 2023, **40**, 100919.

52 I. Tyraskis, A. Capa, G. Skorikova, S. N. Sluijter and J. Boon, Performance optimization of sorption-enhanced DME synthesis (SEDMES) from captured CO_2 and renewable hydrogen, *Front. Chem. Eng.*, 2025, **7**, 1521374.

53 W. H. Chen, B. J. Lin, H. M. Lee and M. H. Huang, One-step synthesis of dimethyl ether from the gas mixture containing CO_2 with high space velocity, *Appl. Energy*, 2012, **98**, 92–101.

54 K. L. Ng, D. Chadwick and B. A. Toseland, Kinetics and modelling of dimethyl ether synthesis from synthesis gas, *Chem. Eng. Sci.*, 1999, **54**, 3587–3592.

55 W. J. Shen, K. W. Jun, H. S. Choi and K. W. Lee, Thermodynamic investigation of methanol and dimethyl ether synthesis from CO_2 hydrogenation, *Korean J. Chem. Eng.*, 2000, **17**, 210–216.

56 J. Hu, Y. Wang, C. Cao, D. C. Elliott, D. J. Stevens and J. F. White, Conversion of biomass syngas to DME using a microchannel reactor, *Ind. Eng. Chem. Res.*, 2005, **44**, 1722–1727.

57 A. T. Aguayo, J. Erena, D. Mier, J. M. Arandes, M. Olazar and J. Bilbao, Kinetic modeling of dimethyl ether synthesis in a single step on a CuO-ZnO-Al_2O_3/γ-Al_2O_3 catalyst, *Ind. Eng. Chem. Res.*, 2007, **46**, 5522–5530.

58 J. Erena, I. Sierra, M. Olazar, A. G. Gayubo and A. T. Aguayo, Deactivation of a CuO-ZnO-Al_2O_3/γ-Al_2O_3 catalyst in the synthesis of dimethyl ether, *Ind. Eng. Chem. Res.*, 2008, **47**, 2238–2247.

59 M. De Falco, M. Capocelli and A. Basile, Selective membrane application for the industrial one-step DME production process fed by CO_2 rich streams: Modeling and simulation, *Int. J. Hydrogen Energy*, 2017, **42**, 6771–6786.

60 G. Jia, Y. Tan and Y. Han, A comparative study on the thermodynamics of dimethyl ether synthesis from CO hydrogenation and CO_2 hydrogenation, *Ind. Eng. Chem. Res.*, 2006, **45**, 1152–1159.

61 P. Styring, P. W. Sanderson, I. Gell, G. Skorikova, C. Sánchez-Martínez, G. García-García and S. N. Sluijter, Carbon footprint of Power-to-X derived dimethyl ether using the sorption enhanced DME synthesis process, *Front. Sustain.*, 2022, **3**, 1057190.

62 V. Dikić, L. Zubeir, M. Sarić and J. Boon, Stripping enhanced distillation—A novel application in renewable CO_2 to dimethyl ether production and purification, *Separations*, 2023, **10**, 403.

63 H. G. Graaf, P. J. J. M. Sijtsema, E. J. Stamhuis and G. E. H. Joosten, Chemical equilibria in methanol synthesis, *Chem. Eng. Sci.*, 1986, **41**, 2883–2890.

64 S. P. Naik, T. Ryu, V. Bui, J. D. Miller, N. B. Drinnan and W. Zmierczak, Synthesis of DME from CO_2/H_2 gas mixture, *Chem. Eng. J.*, 2011, **167**, 362–368.

65 F. Dadgar, R. Myrstad, P. Pfeifer, A. Holmen and H. J. Venvik, Catalyst deactivation during one-step dimethyl ether synthesis from synthesis gas, *Catal. Lett.*, 2017, **147**, 865–879.

66 A. García-Trenco and A. Martínez, The influence of zeolite surface-aluminum species on the deactivation of CuZnAl/zeolite hybrid catalysts for the direct DME synthesis, *Catal. Today*, 2014, **227**, 144–153.

67 J. Boon, J. Van Kampen, R. Hoogendoorn, S. Tanase, F. P. F. van Berkel and M. Van Sint Annaland, Reversible deactivation of Γ-alumina by steam in the gas-phase dehydration of methanol to dimethyl ether, *Catal. Commun.*, 2019, **119**, 22–27.

68 G. H. Graaf, E. J. Stamhuis and A. A. C. M. Beenackers, Kinetics of low-pressure methanol synthesis, *Chem. Eng. Sci.*, 1988, **43**, 3185–3195.

69 G. Berčič and J. Levee, Intrinsic and global reaction rate of methanol dehydration over γ-Al_2O_3 pellets, *Ind. Eng. Chem. Res.*, 1992, **31**, 1035–1040.

70 K.-M. Kim, H. T. Oh, S. J. Lim, K. Ho, Y. Park and C. H. Lee, Adsorption equilibria of water vapor on zeolite 3A, zeolite 13X, and dealuminated Y zeolite, *J. Chem. Eng. Data*, 2016, **61**, 1547–1554.

71 E. Gabruś, J. Nastaj, P. Tabero and T. Aleksandrzak, Experimental studies on 3A and 4A zeolite molecular sieves regeneration in TSA process: Aliphatic alcohols dewatering-water desorption, *Chem. Eng. J.*, 2015, **259**, 232–242.

72 J. van Kampen, J. Boon and M. van Sint Annaland, Steam adsorption on molecular sieve 3A for sorption enhanced reaction processes, *Adsorption*, 2021, **27**, 577–589.

73 F. Dalena, A. Senatore, A. Marino, A. Gordano, M. Basile and A. Basile, *Methanol Production and Applications: An Overview, in Methanol: Science and Engineering*, Elsevier B.V., 2018, pp. 3–28.

74 C. Peinado, D. Liuzzi, M. Retuerto, J. Boon, M. A. Pena and S. Rojas, Study of catalyst bed composition for the direct synthesis of dimethyl ether from CO_2-rich syngas, *Chem. Eng. J. Adv.*, 2020, **4**, 100039.